Acta Geotechnica
https://doi.org/10.1007/s11440-021-01156-2

RESEARCH PAPER

Evaluating scale effects and bearing portions in centrifuge modeling of helical anchors: sand

Ali Akbar Heshmati Rafsanjani[1] · Hossein Salehzadeh[1] · Hamed Nuri[1]

Received: 11 June 2020 / Accepted: 4 February 2021

Abstract

Helical anchors are bearing elements that can resist uplift loads by a combination of shaft and helical plate bearing. The application of helical piles as offshore wind turbine foundations has recently become interesting. However, large size of such structures limits the possible physical modeling in a geotechnical centrifuge. In the current study, the limits of physical modeling concerning particle size effect on the uplift capacity of helical piles were evaluated. The modeling of models technique was employed. The contribution of the shaft and helical plate to the anchor uplift capacity was also studied. The results indicate that small ratios of helical plate diameter to shaft diameter lead to higher contribution of the shaft to the total anchor capacity. It was also found that scale effects could be safely ignored if effective helical radius to the mean grain size of the sand is greater than 16. The normalized mobilization distance and dimensionless breakout factor were in good agreement with the previous researches. The limits reported here could contribute to a more reliable physical modeling of helical piles and anchors in the future researches.

Keywords Breakout factor · Centrifuge modeling · Helical anchor · Mobilization distance · Particle size effect · Scale effects

Abbreviations

A_h	Net projected helical plate area
B	Square plate anchor or footing width
C	Cohesion
C_c	Coefficient of curvature
C_u	Coefficient of unity
COV	Coefficient of variation
D_r	Relative density
D	Helical plate diameter
d	Shaft diameter
d_{50}	Mean grain size
e_{min}	Minimum void ratio
e_{max}	Maximum void ratio
g	Gravitational acceleration
G_s	Specific gravity of solid particles
H	Embedment depth
N_{qu}	Dimensionless breakout factor
P	Pitch of the helical plate
Q_{h-i}	Helical plate tensile load at the moment i
Q_i	Helical anchor tensile load at the moment i
Q_U	Ultimate uplift capacity of the helical anchor
Q_S	Ultimate mobilized shaft bearing
Q_H	Ultimate uplift bearing of the helical plate
$Q_{H(0.1D)}$	Helical plate bearing corresponding to 0.1D displacement
$Q_{H(0.15D)}$	Helical plate bearing corresponding to 0.15D displacement
$Q_{H(1D)}$	Helical plate bearing corresponding to 1D displacement
U_{peak}	Displacement at peak load
W	Effective helical radius
γ'	Effective unit weight of soil
φ	Angle of internal friction, degree
δ_f	Displacement at failure

✉ Ali Akbar Heshmati Rafsanjani
heshmati@iust.ac.ir

Hossein Salehzadeh
salehzadeh@iust.ac.ir

Hamed Nuri
nuri_hamed@civileng.iust.ac.ir

[1] School of Civil Engineering, Iran University of Science and Technology (IUST), Narmak, Tehran, Iran

Published online: 12 April 2021

1 Introduction

Helical piles are bearing elements that comprise a central shaft and one or more helical plates welded to it. These types of bearing elements are also called screw pile/anchor, screw pier, helix anchor, Tsubasa pile and steel rotational pile [34, 47]. A recent application of helical piles as offshore foundation for wind turbines was proposed by [45]. This application has gained much attention as many researchers have conducted tests in this regard such as [6, 27, 43, 46, 58]. The advantages of helical piles as offshore wind turbine foundations include less disturbance for marine life and ease of recycling, according to [47].

Helical piles can resist both compression and tension loads. Several researchers have conducted experiments regarding helical piles such as [11, 16–18, 21, 22, 24, 28, 31, 35, 39, 44, 52, 55, 56, 58, 60]. Among all the available techniques of modeling, centrifuge modeling is a reliable and relatively cost-effective method that has been implemented successfully by many researchers to study helical anchors. Nevertheless, the obtained results using centrifuge testing can be misleading, if scale effects are overlooked. Scale effects exist due to the similarity of the shear band mobilized on the prototype and model interface in terms of thickness, while the sizes of the model and prototype are not similar [4]. Therefore, it is necessary to ensure that the scale effects are minimized in the results of centrifuge testing of helical anchors.

Single-helix anchors resist uplift loads by a combination of shaft bearing and plate resistance. The bearing portion of the shaft is usually ignored if plate-to-shaft diameter ratio (D/d) is large enough. Schiavon [40] performed centrifuge tests on helical anchors with D/d = 3.3 and stated that the shaft portion of the total bearing was less than 22%. Gavin et al. [15] performed in situ tests of helical piles in dense sand and reported that for the D/d = 3.6, the majority of the axial resistance of the pile was provided by the helical plate. Ullah et al. [58] performed tests on helical piles with D/d = 4 in NC clay and reported that shaft bearing contribution to the pile bearing capacity was negligible. However, the shaft and helix bearing portion for lower ratios of D/d is less studied. Moreover, small D/d ratios are more suitable for the offshore environment from a structural point of view [2]. Since helical anchor's capacity is combined of two parts, i.e., shaft bearing and plate bearing, scale effects should be investigated for both portions independently. In this paper, the results of a series of centrifuge tests are presented to evaluate scale effects in the testing of single-helix helical anchors in sand, as well as to determine the contributions of the shaft and plate to the total load bearing of the anchor.

2 Previous studies on scale effects in centrifuge modeling of anchors and footings

There are very limited studies on the scale effects influencing the helical anchors modeling. Many of the previous researchers investigating the scale effects in modeling of geotechnical structures have used the ratio of B/d_{50}, where B is the diameter of the shaft or anchors or width of the footing, etc. and d_{50} is the mean grain size of the tested soil. A summary of previously conducted tests on scale effects is presented below. The studies are categorized based on the installation and modeling conditions, consisting of single-gravity and macro-gravity conditions.

2.1 Single-gravity condition studies

Baker and Kondner [3] performed anchor pullout tests in 1 g conditions in sandy soil to study the scale effects on the uplift capacity of the anchors. Model anchors were circular plates of diameter 25 to 76 mm. The results indicated that scale effects did not substantially influence the uplift capacity in shallow embedment of the anchors. However, as embedment was increased, the scale effects influenced the results considerably. Ovesen [33] installed and tested plate anchors in dense sand in 1 g to 50 g gravity conditions and reported that results were not influenced by scale effects for $B/d_{50} > 25$. Dickin and Leung [10] installed plate and continuous anchors in dense sand in single-gravity conditions and reported no scale effects influencing the peak load for $B/d_{50} > 48$ (B is the anchor width). Tagaya et al. [48] performed centrifuge tests on plate anchors in dense Ottawa sand. The anchors were installed in single-gravity conditions. The authors observed that no scale errors were present for $B/d_{50} > 66$–100. Similar observation to [3] was reported concerning the effect of embedment on the uplift capacity of the anchors. Fioravante [13] conducted centrifuge experiments on shaft models to study the scale effects on the shaft friction mobilization. The author installed the shaft models in the soil in 1 g conditions and then tested the models in the increased gravity conditions. Limits of the safe modeling with respect to the scale effects were reported to be $d/d_{50} > 30$–50. Sakai and Tanaka [38] studied scale effects on the uplift capacity of buried anchors using 1 g laboratory tests and finite element (FE) simulations. The authors tested model anchors with B/d_{50} = 312, 625, 937 in loose, medium and dense sand and reported no scale effects for the anchors installed in medium sand. However, scale effects were observed in the results of anchors installed in dense sand bed.

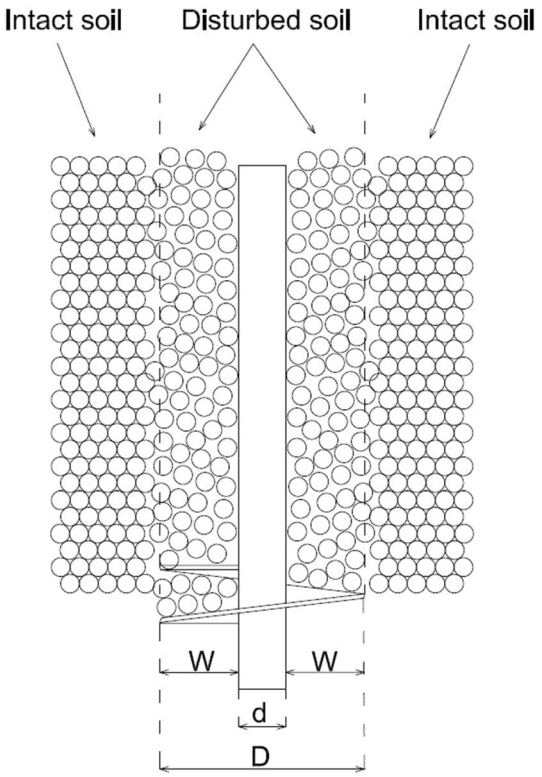

Fig. 1 Effective helical radius W defined in [42]

2.2 Macro-gravity condition studies

Lau [23] performed 1 g and Ng (centrifuge) tests on model footings to evaluate particle size effects on the Terzaghi footing capacity factors and reported that no serious scale effects were observed for footings with $B/d_{50} > 166$–8333. Tatsuoka et al. [51] studied bearing capacity of model footings on granular material and reported no scale effects influencing the results for $B/d_{50} > 33$–50. Toyosawa et al. [53] conducted centrifuge experiments on model footings on river sand to study the influence of scale effects and embedment ratio on the bearing capacity of the prototype footing. Their results suggested that bearing capacity of the prototype footing is the same, if B/d_{50} is greater than 50, for all tested embedment ratios. Even though previous studies have outlined the limiting ratios of d/d_{50} for physical modeling of anchors and footings, this ratio cannot be accurate to evaluate scale effects in helical anchors modeling, as pointed out in [42]. These authors conducted centrifuge tests on single-helix anchors in very dense sand to evaluate the scale effects in the modeling of helical anchors. They stated that since helical anchors vary in the ratio of shaft diameter to plate diameter, the net projected area of the plate is different for each model and therefore, d/d_{50} or D/d_{50} might not be the best parameter to evaluate the particle size effect. They proposed to correlate the bearing resistance of the anchor to the particle size effect by using effective helical radius W. Effective helical radius W (Fig. 1) is defined as $W = 0.5(D - d)$ where d and D are the shaft and helical plate diameters, respectively. They reported that in the ratio of $D/d = 3.3$, particle size effects were negligible for $w/d_{50} > 58$.

Since scale effects in the modeling of helical anchors are only evaluated in the mentioned D/d ratio, it is necessary to establish a rigorous database to encompass all types of helical anchors with different D/d ratios. Any changes in the D/d ratio would result in different bearing portions of the shaft and helical plate of the anchor. Therefore, the present study is focused on I: quantifying the bearing portions of the shaft and plate in a single-helix helical anchor with $D/d = 2$ and II: evaluating the influence of scale effects on the helical anchor bearing in the range of W/d_{50} tested.

3 Equipment

The tests were performed using the beam centrifuge at Geotechnical Engineering Research Center (GERC) at Iran University of Science and Technology (IUST), capable of reaching 200 g with a maximum payload of 14 ton-g. The centrifuge is used for many studies such as those conducted by [5, 36, 37]. To achieve the aims of this research, four model anchors with one helical plate and four model shafts without a helical plate (shaft-only) were fabricated with different dimensions to model the same prototype at different g-levels. This technique is known as modeling of models, explained in detail in [26]. The shaft-only models were used to measure the contribution of the shafts to the total bearing of the anchors. The anchors were installed in medium-dense Firoozkooh sand. The uplift capacity of each model was tested twice to ensure the reproducibility and repeatability of results.

3.1 Tested soil

The soil used in experiments was #161 Firoozkooh silica sand. Several researchers such as [5, 32, 36] have reported the properties of this sand. Mirzaeifar et al. [29] evaluated the mechanical properties of Firoozkooh sand in loose, medium and dense conditions using small-scale direct shear tests. The Firoozkooh sand has a mean grain size (d_{50}) of 0.25 mm, and the angle of internal friction is measured 35 degrees at a relative density of $D_r = 60\%$. The properties of the soil are given in Table 1. The grain size distribution of the sand is shown in Fig. 2 as well.

The sand samples were prepared by pluviating dry sand into the rectangular container with dimensions of 550 × 280 × 250 mm (Length × Width × Height). The dimensions of the container box and model anchors were

Table 1 Mechanical and physical properties of #161 Firoozkooh sand ($D_r = 60\%$)

USCS grade	C_c	C_u	d_{50} (mm)	e_{min}	e_{max}	G_s	C (kPa)	φ
SP	0.88	1.87	0.25	0.55	0.87	2.658	0	35

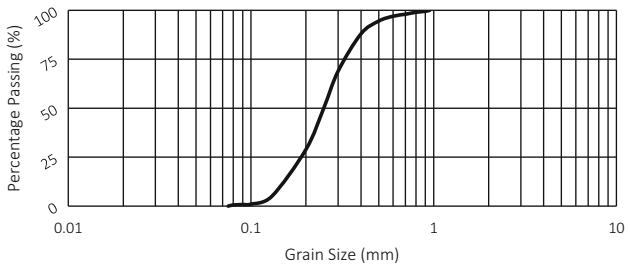

Fig. 2 Grain size distribution of the #161 Firoozkooh sand

Fig. 3 Calibration box being unearthed from the bottom of the sample

selected according to design charts proposed by Ullah et al. [59] to minimize the lateral boundary effects. The container size allowed two models to be tested in each sand sample. The minimum spacing between the tested models was 200 mm. The sand was pluviated into the container in 2-cm steps, having a constant falling height in each step to ensure vertical and horizontal uniformity of the entire sample. A small round calibration box was placed at the bottom of each sample to measure the density and compare the similarity of all the tested samples. Figure 3 illustrates the calibration box being unearthed from the bottom of a tested sample. The results of density measurements and unit weight of the samples are presented in Table 3. The difference in density measurements of each model was less than 3%.

3.2 Loading actuator and test system

A 1-D linear actuator was designed and fabricated to axially test the anchors in flight, based on the limitations of size and loading of the centrifuge facility. The actuator can exert both monotonic compression and tension forces on model piles and anchors in strain-controlled conditions. The actuator consists of a stepper motor, a pulley to transport stepper motor motion to the ball screw and a ball-screw system to transform rotational motion of the motor into the linear motion. A SEWHA-CNM SM603 load cell was connected to the actuator screw tip, capable of measuring 20 kg with a resolution of 0.3 N. The load cell was then connected to the anchor head using a small connecting part, made of aluminum. The actuator was fixed to the sample container by a U-profile and a metal fix, as shown in Fig. 4. The actuator and its connection to the load cell and helical anchor model are also shown in Fig. 4. Because the space for LVDT was limited, an alternative method was used to record the displacements of the anchor. Displacements of the anchor head were recorded indirectly by converting the rotational movement of the ball-screw system to the linear movement. Since all parts are firmly connected using screws and nuts, the recorded displacements show the anchor head displacement. The converting ratio was calibrated using a digital caliper before each test. An automatic Data Acquisition System (DAQ) was fabricated and mounted on the centrifuge swinging basket. DAQ is able to record the data of displacement, force and time with a 40 Hz frequency.

3.3 Helical anchor models

Due to the small ratio of D/d, the weight of the anchor shaft can be significant in small g-levels, when using modeling of models technique. Therefore, aluminum was chosen as the modeling material to fabricate all model anchors. The model anchors consisted of a round aluminum shaft connected to a steel helical plate. A narrow groove with a pitch and width similar to the pitch and thickness of the helical plate was carved into the shaft so that the plate could be fixed to the shaft. The prepared groove was then filled with a very strong epoxy to ensure a firm connection between the shaft and the plate. Special care was given to ensure no extra epoxy remained on the surface of the shaft and plate. The reason for using such connection was to avoid welding because this creates heterogeneous plate surface and therefore influences the plate-sand interface [54]. Four anchors were fabricated with different D and d to model the same prototype with d = 150 mm and D = 300 mm. All the anchors were embedded at H = 6D (H = 1800 mm) to simulate the deep behavior of anchors [50]. The g-level

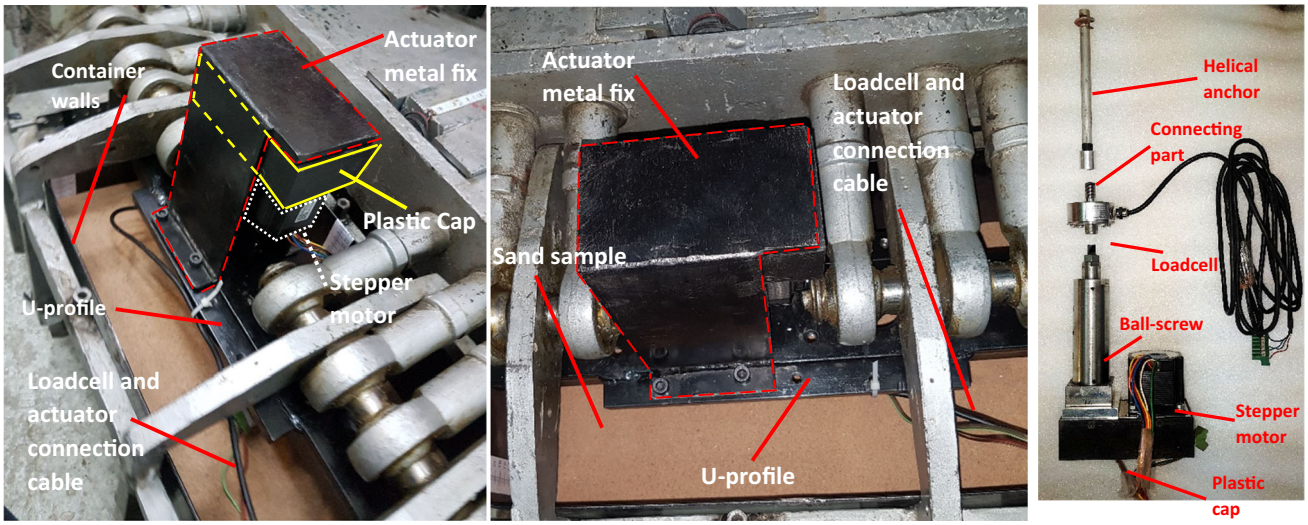

Fig. 4 Prepared sample with the actuator connected to the anchor

was different for each model and was obtained using scaling laws, according to [19]. Model specifications and dimensions are detailed in Table 2. It should be noted that the g-level was calculated for each model according to the depth of the helical plate (the depth of the helical plate corresponds to the middle of the pitch). Because in contrast to centrifuge modeling of conventional straight shaft piles, the effective stress level reproduction is considered for the helical plate rather than the entire shaft. The helical anchor models are shown in Fig. 5.

3.4 Installation and pullout procedure

The anchors were installed in 1 g conditions due to low headroom to operate the in-flight installation. Though, extra measures were taken to model the installation procedure and its effects on the uplift resistance of the anchors. At first, the anchors were installed in perfect installation conditions, i.e., the anchor advancement rate into the soil was one pitch per revolution. This was achieved by installing the anchors using a specially designed installation instrument, having the same pitch as the model anchor. The instrument was fixed to the box to ensure that anchors were vertical during the installation process. After the installation was completed, the sample and the installed anchor were spun at target centrifugal acceleration to let the anchor and its surrounding disturbed soil settle due to increased gravity. This was done to make sure negative friction along the shaft and stress concentration above the helical plate was avoided. The samples were spun at target acceleration for at least three minutes, and then the centrifuge was stopped to mount the actuator and connect the load cell to the anchor head. After assembling the actuator and its components, the centrifuge was again spun at target acceleration for two minutes before the pullout process was started. The load cell recorded the forces continuously from the start of the centrifuge until the prescribed displacement was reached. In order to provide similar initial conditions for all tested models, the forces were reset to zero at the beginning of the pullout process. This made sure no other forces except for the soil shear strength would affect the uplift response of the piles. It should be noted that since the installation was performed in 1 g conditions, one might assume that installation disturbance would be different for different size of the models. However, since all models traversed the soil be their specific pitch, the model soil experienced the same number of cut (screw) cycles during the installation. Therefore, the degree of soil disturbance would be similar in all models and so would be the installation and loading conditions of all models. The anchors were pulled at a vertical displacement rate of 0.25 mm/s at model scale. Figure 6 shows the installation instrument and a model anchor after full penetration into the sand. A schematic view of the loading system and DAQ is presented in Fig. 7.

4 Results

4.1 Shaft bearing portion

To determine the bearing contribution of the shaft and helix for each model anchor, separate centrifuge tests were performed on shaft-only models. The model shafts had the

Table 2 Specifications of model anchors

Model case	Shaft diameter (d) (mm)	Prototype shaft diameter (mm)	Helical plate diameter (D) (mm)	Prototype helical plate diameter (mm)	Plate-to-shaft diameter ratio (D/d)	Helical plate pitch (p) (mm)	Helical plate embedment depth (H) (mm)	Prototype Helical plate embedment depth (mm)	Plate thickness (t) (mm)	Embedment depth ratio (H/D)	g-level (g)
HA-6s12h	6	150	12	300	2	3	72	1800	8	6	25
HA-8s16h	8	150	16	300	2	4	96	1800	10	6	18.75
HA-10s20h	10	150	20	300	2	5	120	1800	10	6	15
HA-12s24h	12	150	24	300	2	5	144	1800	10	6	12.5
SO-6	6	150	–	–	–	–	72	1800	–	6	25
SO-8	8	150	–	–	–	–	96	1800	–	6	18.75
SO-10	10	150	–	–	–	–	120	1800	–	6	15
SO-12	12	150	–	–	–	–	144	1800	–	6	12.5

same shaft diameter as the helical anchor models. The specifications of tests on shaft-only models are presented in Table 2. In order to correctly capture the contribution of the shaft for each model anchor, the shaft-only models were installed and pulled out in the same sand sample in which their corresponding helical anchor was tested. Moreover, to assimilate the installation conditions of the shaft-only model to that of the helical model, the shafts were installed in the sand using the exact same method (pitch-matched installation method) that was used to install their corresponding helical model. For instance, SO-6 mm model was installed using the same advancement rate (pitch) that was used for the installation of HA-6s12h model. Therefore, similar installation conditions were provided for the shaft-only and helical anchor models. It is worth mentioning that such method of determining shaft and helices contribution was previously employed in [55] to specify the contribution of helical plates and shaft to the uplift bearing and installation moment of the anchors. The results of bearing portions of the shaft and helical plate for all tested model anchors are presented in Table 3. The load–displacement graphs of the tested shafts are presented in Fig. 8. It can be seen in Fig. 8 that scale effects partially influence the shaft mobilized resistance as d/d_{50} for the shaft models varies between 24 and 48. According to [13], the influence of scale effects on the shaft friction can be safely avoided if d/d50 is greater than 30–50. However, this effect is limited for the tested shafts with d/d50 > 32 as similar results are gained for shaft models with different sizes. It is evident from Table 3 that bearing portion of the shaft in all tested models can be as high as 30 to 40% of the total bearing of the helical anchor. Small D/d ratios have large shaft frictional surface, and therefore, the shaft bearing portion would be considerable compared to helical anchors with larger D/d ratios (i.e., $D/d > 4$), as [25] has shown. Lutenegger [25] reported an increase in shaft contribution to the total anchor capacity with a decrease in D/d ratio in sands and clays. Schiavon et al. [41] conducted tension field tests on single-helix (with wing ratio $D/d = 3$) and multi-helix piles (tapered with four helices) in clayey sand of Brazil. They observed 0.12 Q_u to 0.37 Q_u shaft contribution for single-helix piles, while a shaft contribution of 0.14 Q_u to 0.52 Q_u was reported for multi-helix piles. They attributed the difference in shaft contribution to the horizontal variability in the soil strength. Cerfontaine et al. [7] performed FE analyses to optimize screw anchors for the offshore environment. They validated FE model against centrifuge experiments for helical anchor of $D/d = 2$ installed to a depth of $H/D = 7.4$ in dense sand. The authors reported a 38% to 46% shaft contribution to the total anchor uplift capacity as the anchor pullout started until reaching a normalized displacement of 0.3D. [20] observed an increase in shaft contribution as a result of

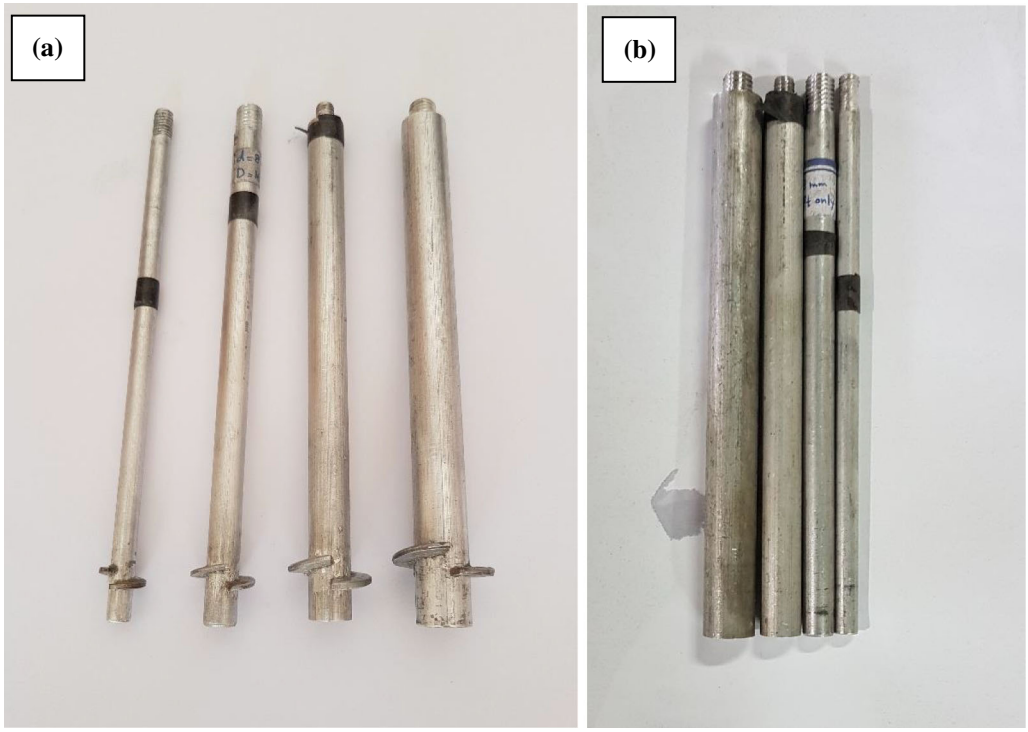

Fig. 5 Physical models of (**a**): helical anchors and (**b**): shaft-only

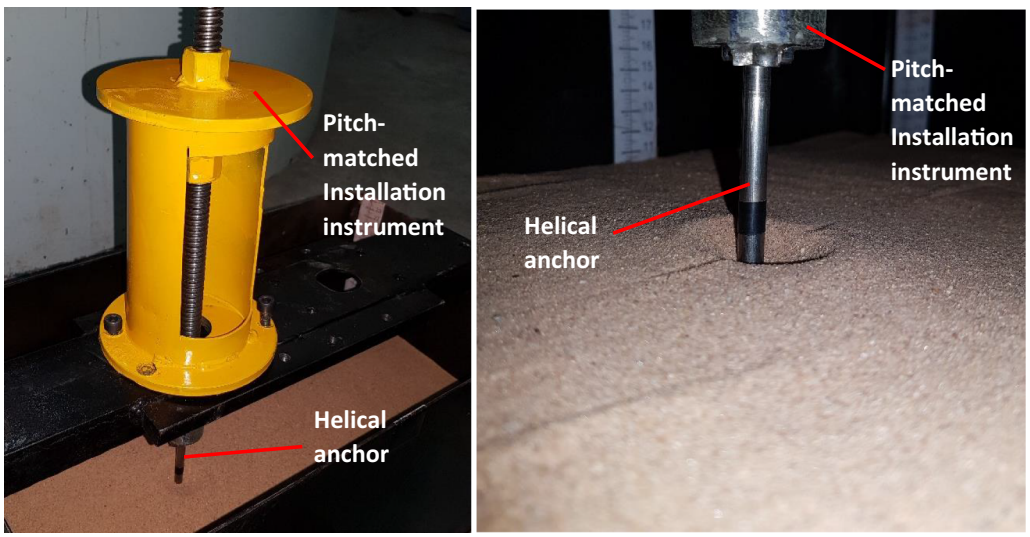

Fig. 6 Model anchor after full penetration into the sand using pitch-matched installation instrument

helical blade size and D/d decrease. [30] conducted laboratory small-scale tests on helical anchors with $1.5 < D/d < 3$ and showed that shaft bearing contributes to a large portion of the helical anchor uplift capacity in the tested models. Filho and Tsuha [12] installed single-helix and double-helix anchors with wing ratio (D/d) of 3.77 in tropical residual soil of sandstone and reported a 30% of shaft bearing portion for the single-helix anchor.

Thus, contrary to helical anchors with large D/d ratios ($D/d > 4$), the shaft bearing contribution to the ultimate bearing of the anchors with small D/d ratios ($D/d = 2$ in this case) cannot be overlooked and shaft bearing should be taken into account for proper capacity prediction, because failing to do so would result in underestimation of the anchor capacity, leading to increased costs of construction and maintenance. This is particularly important in the offshore application of helical piles, where piles are usually

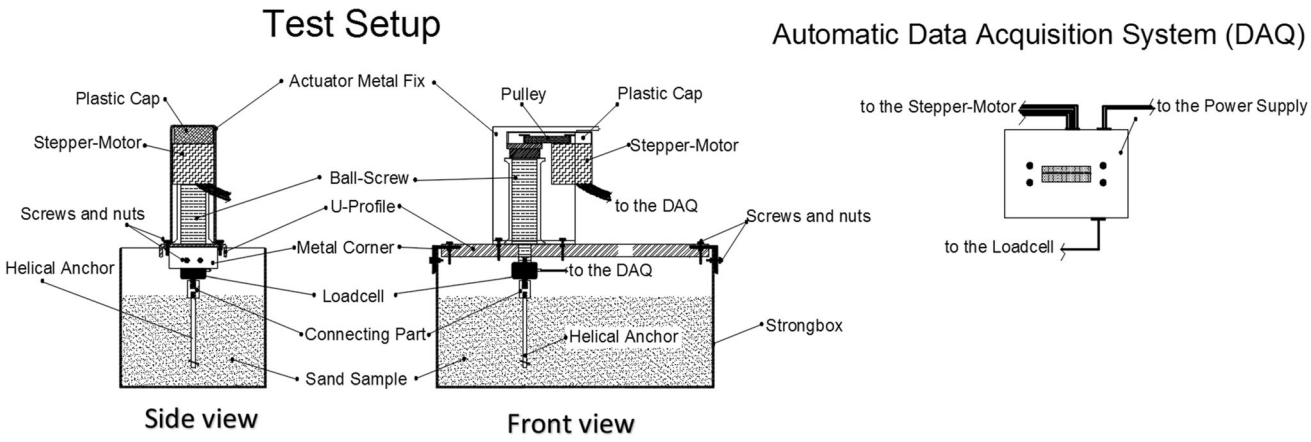

Fig. 7 Schematic view of the actuator and data acquisition system (DAQ)

Table 3 Relative density of soil samples and bearing portions of the shaft and helical plate for tested models (prototype scale)

Model case	Mean sample unit weight (kN/m^3)	Mean relative density	Ultimate uplift capacity of helical anchor (Q_U) kN	Ultimate mobilized shaft bearing (Q_s) kN	%	Ultimate uplift bearing of helical plate (Q_H) kN	%
HA-6s12h	15.71	63%	44.7	15.7	35	29	65
HA-8s16h	15.76	65%	28.7	10.6	37	18.1	63
HA-10s20h	15.59	59%	22.8	7.5	33	15.3	67
HA-12s24h	15.55	57%	23.9	7.4	31	16.5	69
HA-6s12h-R	15.77	65%	43.2	15.6	36	27.6	64
HA-8s16h-R	15.64	60%	28.9	10.5	36	18.4	64
HA-10s20h-R	15.70	62%	29	11.3	39	17.7	61
HA-12s24h-R	15.75	64%	31.4	11.8	37	19.6	63
Average	15.68	62%	–	–	35.5	–	64.5

installed in shallow conditions due to limitations of installation equipment [47] and shaft contribution could be significant in this case.

Therefore, shaft contribution is remarkable in the tested helical anchors ($(0.3 \sim 0.4)Q_U$). However, more research is needed to determine the more exact shaft bearing contribution to the anchor capacity in small D/d ratios without scale effects influencing the results.

4.2 Scale effects

The load–displacement curves of centrifuge tests on helical anchors in prototype values are presented in Fig. 9. The anchors were pulled until a displacement of 1D was reached (D is the helix diameter).

Figure 9 shows that scale effects are not negligible in the models tested, as the ultimate bearing of the models is considerably different. The largest peak uplift capacity is twice that of the smallest. The mean ultimate tensile load measured in eight tests is 31.3 kN with a standard deviation of 8.2 kN and a coefficient of variation (COV) of 26%. This is because the scale effects are known to affect the results in shaft models of $d/d_{50} < 30$–50 according to [13] and $d/d_{50} < 100$ according to [14]. There is debate on the ratio of d/d_{50} beyond which scale effects are negligible for shaft frictional bearing. However, in $d/d_{50} < 30$–50 most probably results are partially influenced by scale effects.

Therefore, to better evaluate scale effects in modeling of helical anchors, the shaft bearing and plate bearing were separated for each model. The helical plate load–displacement curve was obtained using Eq. (1):

$$\frac{Q_{h-i}}{Q_i} = \frac{(Q_U - Q_S)}{Q_U} \tag{1}$$

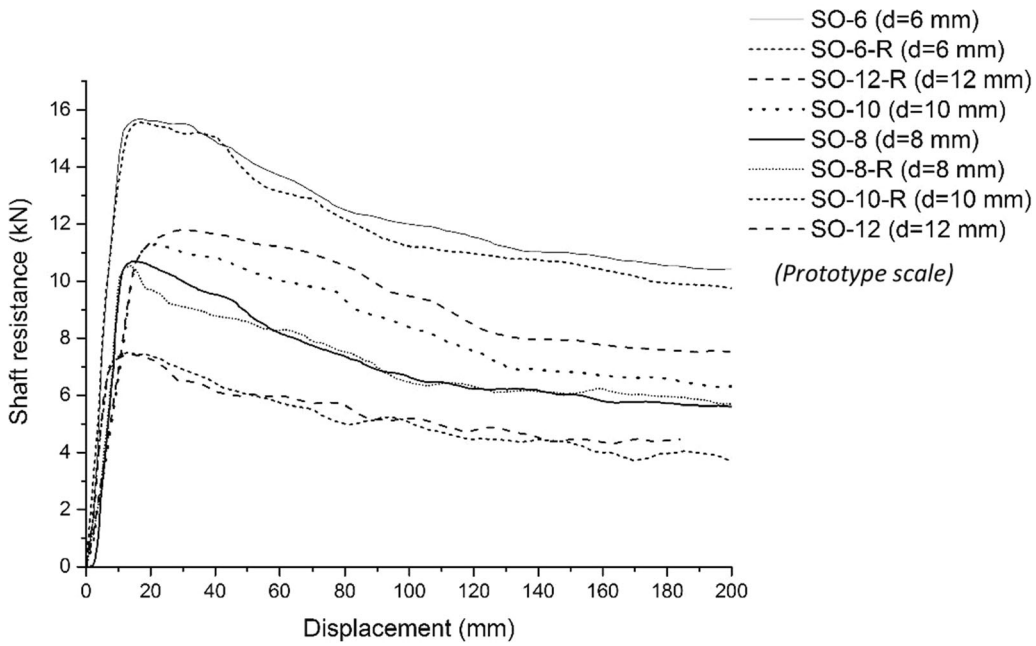

Fig. 8 Load–displacement curves for shaft-only models. (Prototype scale)

where Q_{h-i} is helical plate tensile load at the moment i, Q_i helical anchor tensile load at the moment i, Q_U ultimate uplift capacity of the helical anchor, Q_S ultimate mobilized shaft bearing.

The load–displacement curves of a typical helical plate and helical anchor are demonstrated in Fig. 10. Because model shaft and model helical anchor have different stiffness values (i.e., the gradient of the load–displacement curve in the linear region) due to different required displacement for capacity mobilization, this equation was used to separate the shaft and helical plate bearing portions. This ensures that the helical plate curve is similar to that of the helical anchor and comparable to other tested models. It is worth mentioning that shaft pullout tests were conducted in the same sand sample as the helical anchor was tested, as two models could be tested in each sample with proper spacing.

The load–displacement curves are presented for shaft-only (d = 8 mm) and helical anchor (D = 16 mm) models in Fig. 11. It can be seen that the net plate bearing curve could not be obtained by simply subtracting the values of the load–displacement curve of the shaft-only from that of helical anchor.

The maximum measured tensile loads for the helical anchor and helical plate are provided in Table 4 separately. The corresponding displacements are also shown along with D/d_{50} and W/d_{50} of all the models. The ultimate uplift capacity of each test is assumed to be the maximum force measured during the test.

Table 4 indicates that the ultimate uplift capacities of model anchors with $D/d_{50} < 64$ or $W/d_{50} < 16$ are remarkably higher than the rest, and even after separating the shaft and helix bearing portions, the scale effects are still present. This trend can be seen in the results of the repeated tests as well, whose assigned names end in "*R*" letter.

The load–displacement curves for plates of the tested anchors are shown in Fig. 12. It is evident from Fig. 12 that scale effects are negligible for plates with $D/d_{50} > 64$ or $W/d_{50} > 16$. As shown in Table 5, models with $W/d_{50} > 16$ have a mean peak load value of 17.6 kN with a standard deviation of 1.5 kN and coefficient of variation (COV) of 8.5%. The minor differences between the results are attributed to the heterogeneity of the samples as no discernable trend relating to scale effects could be detected in the results. The stiffness, peak load and residual load after a displacement of U = 1D are similar for tested models with $W/d_{50} > 16$. However, the results of anchors with W/d_{50} = 12 are considerably higher than the rest in terms of stiffness and peak load and residual load. This is attributed to the presence of scale effects due to larger shear band formed around the model anchor that results in an unrealistic increase in peak load of the helical plates. Figure 12 suggests that scale effects are avoidable in the modeling of helical anchors with $W/d_{50} > 16$; however, special care must be taken to isolate the scale effects in the modeling of the shaft of the helical anchor.

Oscillations were observed in the post-peak behavior of all the tested anchors, as shown in Fig. 12. This is attributed to the infilling of the gap developed beneath the

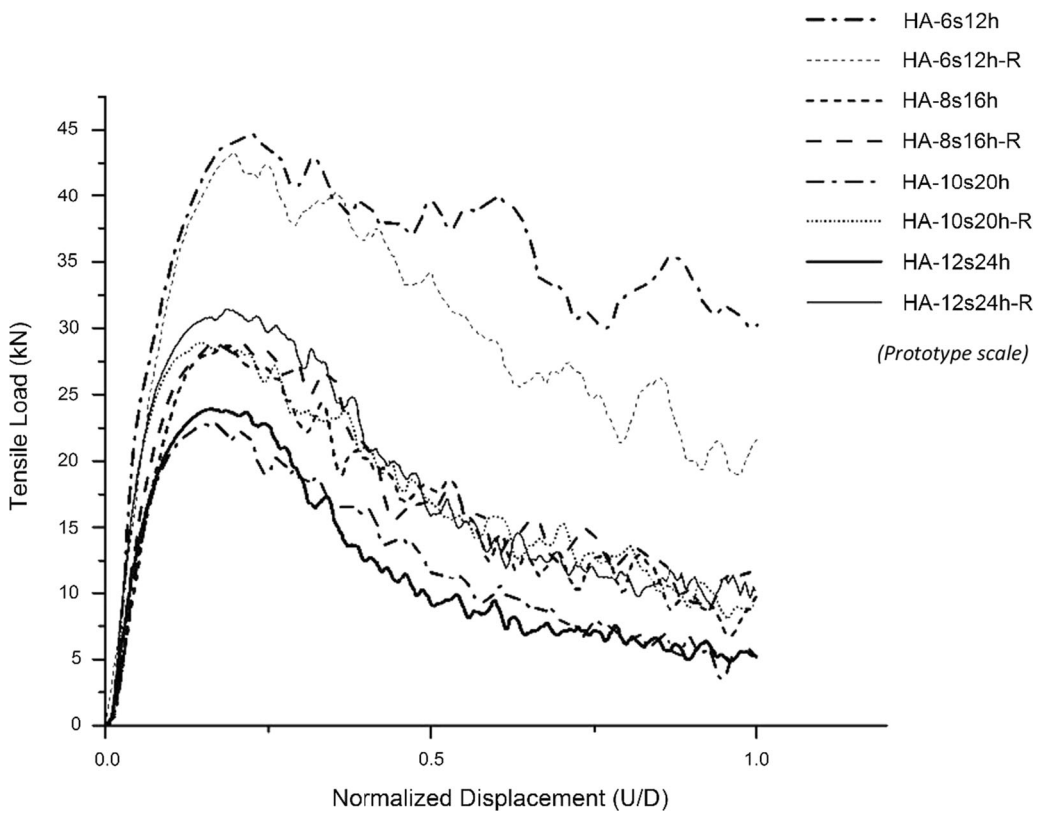

Fig. 9 Load–displacement curves for tested helical anchors. (Prototype scale)

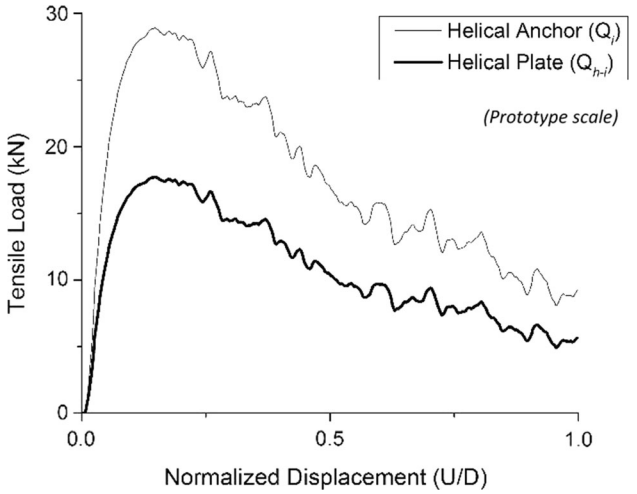

Fig. 10 Load–displacement curve of the helical plate and helical anchor for HA-10s20h-R model. (Prototype scale)

helical plate as the anchor is pulled out, similar to observations in [17]. Also, sample heterogeneity could be responsible for subsequent peaks observed in the load–displacement curves. To verify this phenomenon, the authors are conducting a separate investigation into the failure mechanism of helical anchors under different conditions and the results will be published in separate technical papers.

The obtained values of W/d_{50} and D/d_{50} to avoid scale effects are much inferior to the previously reported studies on helical anchors (e.g., $W/d_{50} > 64$ in [42]). However, the results are in good agreement with findings on modeling of plate anchors. For example, [33] reported critical B/d_{50} to avoid scale effects to be 25 (compared to $W/d_{50} > 16$ or 2 $W/d_{50} > 32$ obtained in the current study). Such small values of $D/d_{50} > 64$ and $W/d_{50} > 16$ are of interest to model the helical piles for offshore applications in a geotechnical centrifuge because these structures are considerably larger than conventional onshore helical piles and the centrifuge modeling of the piles can turn out to be a challenge due to size restrictions. Although some innovative methods can be used to reduce the size of the model, as applied in [8], there is still a challenge for proper modeling of such large structures. Therefore, determining the limits for proper modeling in a geotechnical centrifuge can be of significant value.

4.3 Normalized mobilization distance

According to Table 4, the mean relative displacement required to mobilize the peak uplift capacity was $U_{\text{peak}}/D = 0.17$. This is consistent with normalized

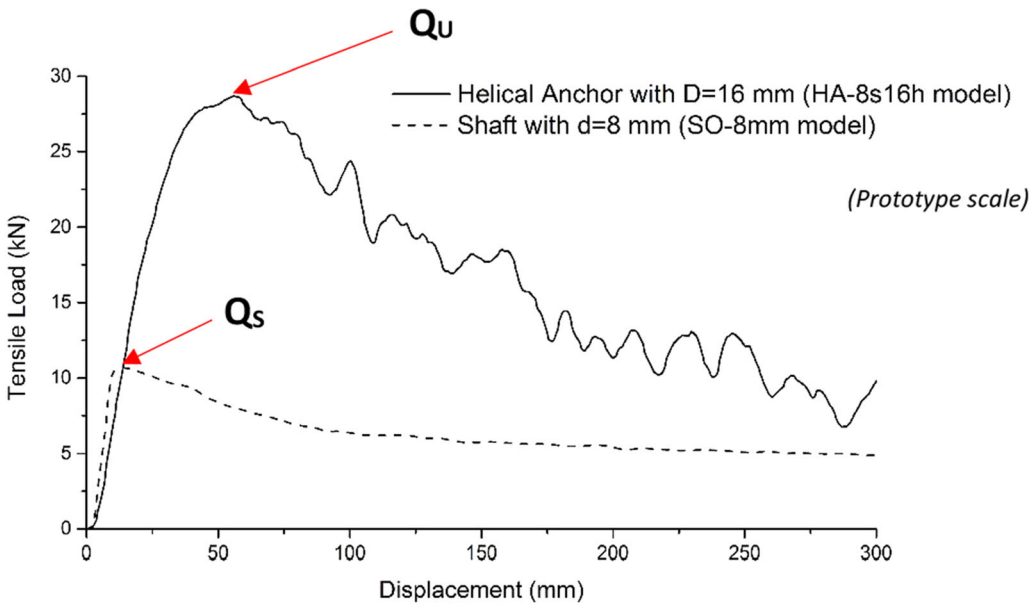

Fig. 11 load–displacement curves for the shaft (d = 8 mm) and helical anchor (D = 16 mm) (Prototype scale)

Table 4 Maximum measured tensile load of helical anchor and helical plate and corresponding displacement of tested models (prototype scale)

Model case	d/d_{50}	D/d_{50}	W/d_{50}	Q_U (kN)	Q_H (kN)	U_{peak} (mm)	U_{peak}/D
HA-6s12h	24	48	12	44.7	29	67.5	0.22
HA-8s16h	32	64	16	28.7	18.1	55.6	0.18
HA-10s20h	40	80	20	22.8	15.3	50.8	0.17
HA-12s24h	48	96	24	23.9	16.5	48.5	0.16
HA-6s12h-R	24	48	12	43.2	27.6	58.7	0.19
HA-8s16h-R	32	64	16	28.9	18.4	51.7	0.17
HA-10s20h-R	40	80	20	29	17.7	44	0.15
HA-12s24h-R	48	96	24	31.4	19.6	56	0.19
Average				31.3	20.3	54.1	0.18

mobilization distance obtained for buried pipelines, proposed by [61] by Eq. (2):

$$\frac{\delta_f}{D} = M \times \frac{H}{D} + N \tag{2}$$

where $M = 0.025$ and $N = 0.009$ for maximum mobilized uplift resistance. It should be noted that Eq. 2 is derived based on the H/D ranges tested in [61] and a deviation from this linear equation was reported for $H/D > 8$ in [17].

This indicates that assuming the anchor capacity is reached after a displacement of 0.1D is not realistic and leads to an underestimation of the anchor uplift capacity in medium-dense sand. Hao et al. [17] performed centrifuge tests on wished in place (WIP) helical anchors and reported that normalized mobilization distance for anchor embedment of H/D = 6 was almost 0.15 in dense sand. Though, it is expected that normalized mobilization distance changes as the soil density and soil particles' physical characteristics including angularity and crushability are altered.

Table 5 presents the load corresponding to 0.1D and 0.15D displacement for each test. Table 5 indicates that the load corresponding to 0.15D displacement represents a better estimation of the peak uplift bearing in the tests performed.

The residual uplift bearing after a displacement of 1D is also shown for each model in Table 5. As shown in Table 5, the mean residual uplift bearing of the plate is almost 30% of the peak uplift resistance ($Q_{H(1D)}/Q_H = 30\%$). Newgard et al. [31] reported 50% to 80% reduction in the monotonic uplift bearing of helical anchors after a displacement of 1D. The decrease in uplift resistance can be attributed to the decrease in soil shear resistance along the shear plane which is calculated using residual friction angle of the soil φ_r, as well as the reduced contact surface area of the model anchor with the surrounding soil and a reduction in embedment depth equal to 1D as the anchor is pulled out.

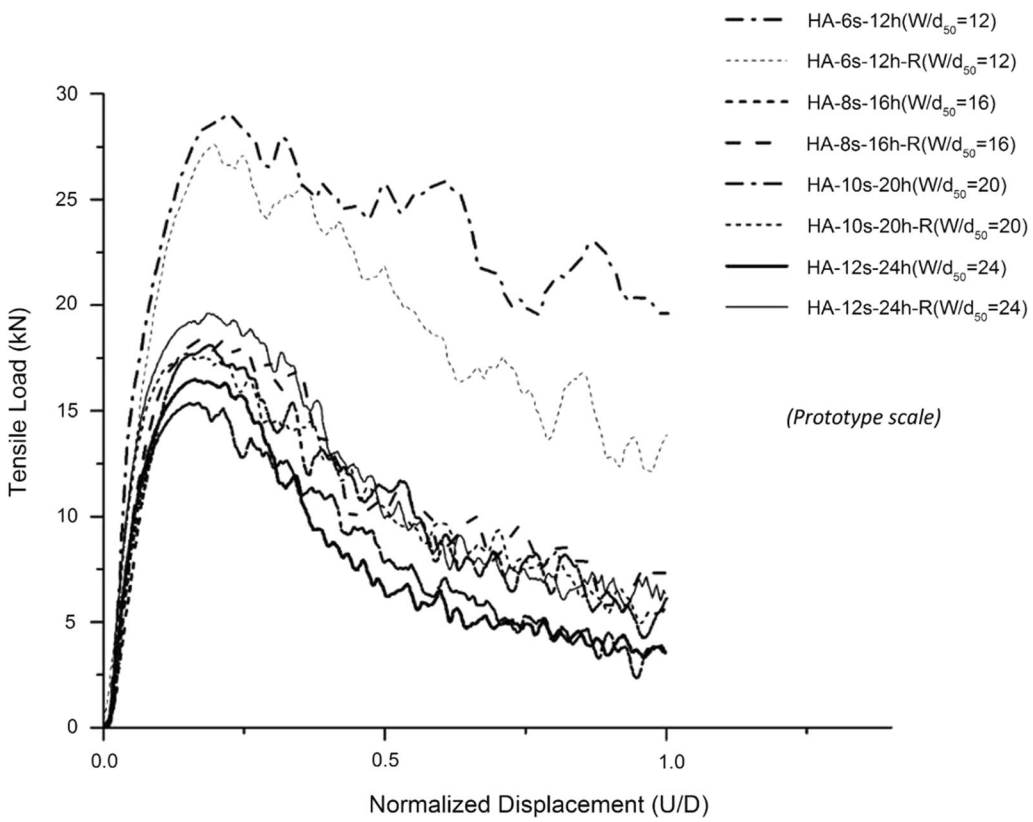

Fig. 12 Load–displacement curves for the helical plates. (Prototype scale)

Table 5 Results of centrifuge tests on helical anchors without scale effects (prototype scale)

Model case	d/d_{50}	D/d_{50}	W/d_{50}	Q_H (kN)	Breakout factor N_{qu}	$Q_{H(0.1D)}$ (kN)	$Q_{H(0.15D)}$ (kN)	$Q_{H(1D)}$ (kN)	$Q_{H(1D)}/Q_H$ %	U_{peak}/D
HA-8s16h	32	64	16	18.1	12.1	14.7	17.6	6.1	34	0.18
HA-10s20h	40	80	20	15.3	12.3	13.9	15.3	3.4	22	0.17
HA-12s24h	48	96	24	16.5	10.3	14.6	16.3	3.6	22	0.16
HA-8s16h-R	32	64	16	18.4	11.8	16	18	7.4	40	0.17
HA-10s20h-R	40	80	20	17.7	11	16.6	17.6	5.6	33	0.15
HA-12s24h-R	48	96	24	19.6	13.1	17.5	19.1	6.4	34	0.19
Average				17.6	11.7	15.6	17.3	5.4	30%	0.17
Standard deviation				1.5	1	1.37	1.34	1.6		
COV				8.5%	8.5%	8.8%	7.7%	29%		

4.4 Breakout factor in deep conditions N_{qu}

Adams and Klym [1] were among the first to use a dimensionless breakout factor to calculate the uplift resistance of helical anchors. They conducted experiments on various soil types (granular and cohesive) and used N_{qu} factor that was based on the angle of friction and relative density for the granular soils. There have been many researches ever since to determine the breakout factor in different conditions and parameters effecting it. Recently, [17] reported an increase in N_{qu} with embedment ratio (H/D) for plate and helical anchors installed in dense to very dense sand. They observed that beyond embedment ratio of $H/D = 9$, the breakout factor was almost constant and concluded that $H/D = 9$ is the limiting depth to ensure deep behavior of the anchor in dense sand. Tsuha et al. [57]

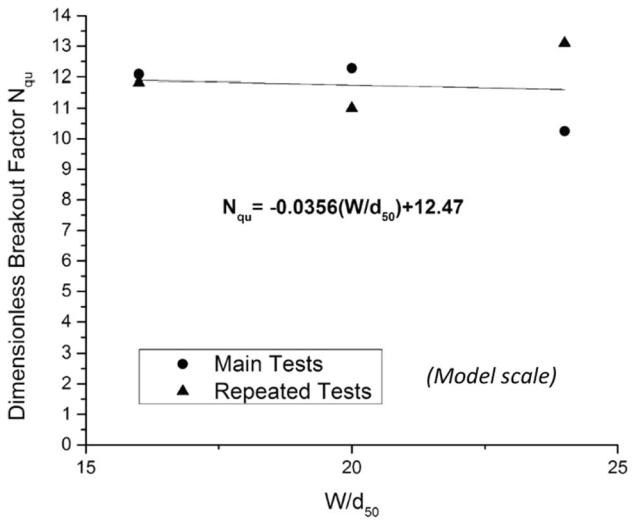

Fig. 13 Dimensionless breakout factor N_{qu} for tested helical plates. (Prototype scale)

evaluated the effect of anchor embedment ratio and helical plate diameter on the measured breakout factor N_{qu} using small-scale centrifuge tests. The results indicated that the embedment ratio had a major influence on the N_{qu} factor, while plate diameter partially affected the N_{qu} factor. The increase in embedment ratio increased the value of N_{qu}, while larger plate diameter resulted in lower breakout factor. Also, the sand relative density was deemed as the most effective parameter on the uplift resistance of helical plates.

In the present study, the breakout factor was obtained for tested anchors using Eq. (3), proposed by Adams and Klym [1], described as:

$$N_{qu} = \frac{Q_H}{\gamma' H A_h} \tag{3}$$

where Q_H is the ultimate uplift bearing of the helical plate (kN), γ' is the effective unit weight of the soil (kN/m^3), H is the embedment depth (m), N_{qu} is the dimensionless breakout factor and A_h is the net projected helical plate surface area (m^2).

Figure 13 presents the results of N_{qu} obtained for all tests, excluding the results containing scale effects. It can be seen in Fig. 13 and Table 5 that N_{qu} values have an average of $N_{qu} = 11.7$ and a COV of 8.5%, indicating that scale effects are avoidable in the results. A mildly decreasing trend line can also be observed as the w/d50 is increased, implying the reduction in breakout factor with the increasing plate size.

The obtained values of N_{qu} are in general agreement with previous findings for plate anchors, e.g., [9, 49]; however, the N_{qu} values are lower than previous researches on helical piles such as [17] where $N_{qu} = 21 \sim 23$ for $H/D = 6$ was reported. There are a few reasons explaining this difference:

Separating the shaft mobilized capacity from the total anchor capacity would decrease the N_{qu} values, since shaft contributes to the total anchor capacity by roughly 30–40 percent (Table 3). This suggests that N_{qu} values for anchors with small D/d could be lower than anchors with larger D/d as shaft contribution is different for each case.

The higher relative density of sand would result in a lower N_{qu} value as a result of disturbance caused by the anchor installation. In the current study, the sand was medium dense and therefore, smaller values of N_{qu} are expected in comparison with recommended values for N_{qu} in previous reports.

Generally, N_{qu} values are smaller in tension compared to that of compression, and it would be more accurate if N_{qu} is calculated based on the disturbed soil friction angle [47]. Therefore, smaller values of N_{qu} should be expected in the estimation of the uplift resistance of the helical anchors in tensile applications compared to compression cases.

5 Conclusion

A total of 16 centrifuge tests were conducted on helical anchors with and without helical plates with different sizes to model the same prototype. The anchors were installed in single-gravity conditions and were then spun at target centrifugal acceleration to replicate the field conditions. The anchors were then pulled to evaluate the presence of scale effects as well as to determine the contribution of the shaft and plate to the anchor ultimate bearing separately. The main findings of this research are:

1. Contrary to helical anchors with large D/d ratios (typically 3 to 5 for onshore helical anchors), the shaft contributes to a large portion of the total anchor capacity ($(0.3 \sim 0.4)Q_U$) in anchors with $D/d = 2$ ratio tested in the current study. Therefore, shaft contribution cannot be overlooked in the uplift bearing of the helical anchor with small D/d ratios.
2. Comparing the load–displacement curve of helical plates reveals that scale effects are negligible for $W/d_{50} > 16$. This ratio becomes particularly useful when modeling helical piles for offshore applications in a geotechnical centrifuge where restrictions of size are considerable. It should be reminded that these results are obtained under specific testing procedures reported

earlier and therefore are subject to further research to ensure the validity of the results.

3. Oscillations observed in the load–displacement curve after reaching the peak load are assumed to be as a result of infilling of the gaps formed beneath the upward moving plate. Similar observations are reported in the uplift mechanism of helical anchors and buried pipelines in the literature. Separate studies should be conducted to confirm such hypothesis.
4. The residual uplift resistance of the anchors was nearly 30% of the peak load after a displacement of 1D. This behavior is attributed to the reduction in mobilized friction angle of the soil as well as reduced contact surface area and embedment depth. It should be noted that this conclusion is drawn for the installation procedure employed in the current study (1-g pitch-matched method).
5. Breakout factor N_{qu} obtained for the current study confirms that scale effects are negligible for $W/d_{50} > 16$. A minor decrease in breakout factor with increased plate size was observed. Also, the N_{qu} values are relatively smaller than the previously reported values for N_{qu} for helical anchors. This is deemed to be as a result of soil disturbance during installation (1-g pitch-matched installation), the direction of exerted loading, sample heterogeneity, as well as considerable contribution of the shaft resistance to the total anchor capacity.

Acknowledgements The third author would like to thank Dr. A. Askarinejad from Delft University of technology and Dr. C.H.C. Tsuha from University of Sao Paulo for their support and contributions to the physical modeling in this research.

Funding The authors declare that no funding was received to perform this research.

Availability of data and materials The data and material presented here are available upon request from the corresponding author.

Code availability No codes or software were used in preparing the results of this research.

Declarations

Conflict of interest The authors declare that they have no conflict of interest.

References

1. Adams JI, Klym TW (1972) A study of anchorages for transmission tower foundations. Can Geotech J 9(1):89–104. https://doi.org/10.1139/t72-007
2. Al-Baghdadi TA, Brown MJ, Knappett JA,Ishikura R (2015) Modelling of laterally loaded screw piles with large helical plates in sand. In: Frontiers in offshore geotechnics III: proceedings of the 3rd international symposium on frontiers in offshore geotechnics (ISFOG 2015), 2015, vol 1. pp 503–508
3. Baker WH, Kondner RL (1966) Pullout capacity of a circular earth anchor buried in sand. Highw Res Rec 108:1–10
4. Bałachowski L (2006) Scale effect in shaft friction from the direct shear interface tests. Arch Civ Mech Eng 6(3):13–28. https://doi.org/10.1016/S1644-9665(12)60238-6
5. Baziar MH, Shahnazari H, Kazemi M (2018) Mitigation of surface impact loading effects on the underground structures with geofoam barrier: Centrifuge modeling. Tunn Undergr Sp Technol 80:128–142. https://doi.org/10.1016/j.tust.2018.06.010
6. Brown MJ,Davidson C, Cerfontaine B, Ciantia M, Knappett J (2019) First Indian symposium on offshore geotechnics (ISOG 2019) developing screw piles for offshore renewable energy application. In: First Indian symposium on offshore geotechnics (ISOG 2019). pp 1–9
7. Cerfontaine B, Knappett J, Brown MJ, Davidson C, Sharif Y (2020) Optimised design of screw anchors in tension in sand for renewable energy applications. Ocean Eng 217(c):108010. https://doi.org/10.1016/j.oceaneng.2020.108010
8. Davidson C, Brown MJ, Brennan AJ, Knappett JA, Cerfontaine B, Sharif YU (2019) Physical modelling of screw piles for offshore wind energy foundations. In: Proceedings of the 1st international screw pile symposium on screw piles for energy applications, Dundee, pp 31–37
9. Dickin EA (1988) Uplift behavior of horizontal anchor plates in sand. J Geotech Eng 114(11):1300–1317. https://doi.org/10.1061/(ASCE)0733-9410(1988)114:11(1300)
10. Dickin EA, Leung CF (1983) Centrifugal model tests on vertical anchor plates. J Geotech Eng 109(12):1503–1525. https://doi.org/10.1061/(ASCE)0733-9410(1983)109:12(1503)
11. Fateh AMA, Eslami A, Fahimifar A (2017) Study of soil disturbance effect on bearing capacity of helical pile by experimental modelling in FCV. Int J Geotech Eng 11(3):289–301. https://doi.org/10.1080/19386362.2016.1222692
12. Filho JMSMdS, Tsuha CdHC (2019) Uplift performance of large - capacity helical piles in a tropical residual soil. In: Proceedings from the XVI Pan-American conference on soil mechanics and geotechnical engineering (XVI PCSMGE 2019), vol. 0. pp 913–920. doi: https://doi.org/10.3233/STAL190129
13. Fioravante V (2002) On the shaft friction modelling of non-displacement piles in sand. Soils Found 42(2):23–33. https://doi.org/10.3208/sandf.42.2_23
14. Garnier J, Konig D (1998) Scale effects in piles and nails loading tests in sand. In: Centrifuge 98. pp 205–210
15. Gavin K, Doherty P, Tolooiyan A (2014) Field investigation of the axial resistance of helical piles in dense sand. Can Geotech J 51(11):1343–1354. https://doi.org/10.1139/cgj-2012-0463
16. Hambleton JP, Stanier SA, Gaudin C, Todeshkejoei K (2014) Analysis of installation forces for helical piles in clay. Australian Geomech 49(4):73–80
17. Hao D, Wang D, O'Loughlin CD, Gaudin C (2019) Tensile monotonic capacity of helical anchors in sand: interaction between helices. Can Geotech J 56(10):1534–1543. https://doi.org/10.1139/cgj-2018-0202
18. Hoyt RM, Clemence SP (1989) Uplift capacity of helical anchors in soil. In: Proceedings of the 12th international conference on soil mechanics and foundation engineering, Rio de Janeiro, Brazil., vol 2
19. Kutter BL (1992) Dynamic centrifuge modeling of geotechnical structures. Transp Res Rec no. 1336
20. Kwon O, Lee J, Kim G, Kim I, Lee J (2019) Investigation of pullout load capacity for helical anchors subjected to inclined loading conditions using coupled Eulerian-Lagrangian analyses. Comput Geotech 111(March):66–75. https://doi.org/10.1016/j.compgeo.2019.03.007

21. Lanyi SA (2017) Behaviour of helical pile groups and individual piles under compressive loading in a cohesive soil, M.Sc Thesis, University of Alberta, Edmonton, Alberta
22. Lanyi-Bennett SA, Deng L (2019) Axial load testing of helical pile groups in glaciolacustrine clay. Can Geotech J 56(2):187–197. https://doi.org/10.1139/cgj-2017-0425
23. Lau C (1988) Scale effects in tests on footings. Ph.D. thesis, University of Cambridge, Cambridge, UK.
24. Li W, Deng L (2018) Axial load tests and numerical modeling of single-helix piles in cohesive and cohesionless soils. Acta Geotech. https://doi.org/10.1007/s11440-018-0669-y
25. Lutenegger AJ (2019) Screw piles and helical anchors–what we know and what we don't know: an academic perspective–2019. In: ISSPEA 2019. p 15
26. Madabhushi G (2015) Centrifuge modelling for civil engineers. CRC Press, London
27. McNamara A (2018) Physical modelling in geotechnics. CRC Press, Boca Raton
28. Merifield RS (2011) Ultimate uplift capacity of multiplate helical type anchors in clay. J Geotech Geoenviron Eng 137(7):704–716. https://doi.org/10.1061/(ASCE)GT.1943-5606.0000478
29. Mirzaeifar H, Abouzar A, Abdi MR (2013) Effects of direct shear box dimensions on shear strength parameters of geogrid-reinforced sand. In: 66th Canadian geotechnical conference and the 11th joint CGS/IAH-CNC groundwater conference. pp 1–6
30. Nagata M, Hirata H (2005) Study on uplift resistance of screwed steel pile. In: Nippon steel technical report no. 92. Tokyo, Japan: Nippon Steel & Sumitomo Metal Corporation., no. 92, pp 73–78
31. Newgard J, Schneider J, Thompson D (2015) Cyclic response of shallow helical anchors in a medium dense sand. In: Frontiers in offshore geotechnics III. CRC Press, pp 913–918
32. Nuri H (2015) Studying the effect of geometric nail layout on the soil-nailed wall behavior, using the Ng modelling. M.Sc. Thesis, Iran University of Science and Technology
33. Ovesen KN (1981) Centrifuge tests of uplift capacity of anchors. In: Proceedings of the 10th international conference on SMEE. pp 717–722
34. Perko HA (2009) Helical piles: a practical guide to design and installation. Wiley, Hoboken . https://doi.org/10.1002/9780470549063
35. Prasad YVSN, Rao SN (1996) Lateral capacity of helical piles in clays. J Geotech Eng 122(November):938–941
36. Sabermahani M, Ahimoghadam F, Ghalehnovi V (2018) Effect of surcharge magnitude on soil-nailed wall behaviour in a geotechnical centrifuge. Int J Phys Model Geotech 18(5):225–239. https://doi.org/10.1680/jphmg.16.00022
37. Saeedi Azizkandi A, Baziar MH, Rasouli H, Modarresi M, Shahnazari H (2015) Centrifuge modeling of non-connected piled raft system. Int J Civ Eng 13(2):114–123. https://doi.org/10.22068/IJCE.13.2.114
38. Sakai T, Tanaka T (2007) Experimental and numerical study of uplift behavior of shallow circular anchor in two-layered sand. J Geotech Geoenviron Eng 133(4):469–477. https://doi.org/10.1061/(ASCE)1090-0241(2007)133:4(469)
39. Sakr M (2015) Retracted: relationship between installation torque and axial capacities of helical piles in cohesionless soils. J Perform Constr Facil 29(6):04014173. https://doi.org/10.1061/(ASCE)CF.1943-5509.0000621
40. Schiavon JA (2016) Experimental investigation on the helical pile behaviour under cyclic tensile loading. University of São Paulo, São Carlos
41. Schiavon JA, Filho JMSMdS, Tsuha CdHC, Thorel L (2015) The occurrence of residual stresses in helical piles. In: Proceedings of the 15th Pan-American conference on soil mechanics and geotechnical engineering. pp 1851–1858. Doi: https://doi.org/10.3233/978-1-61499-603-3-1851
42. Schiavon JA, Tsuha CHC, Thorel L (2016) Scale effect in centrifuge tests of helical anchors in sand. Int J Phys Model Geotech. https://doi.org/10.1680/jphmg.15.00047
43. Spagnoli G (2013) Some considerations regarding the use of helical piles as foundation for offshore structures. Soil Mech Found Eng 50(3):102–110. https://doi.org/10.1007/s11204-013-9219-7
44. Spagnoli G (2017) A CPT-based model to predict the installation torque of helical piles in sand. Mar Georesour Geotechnol 35(4):578–585. https://doi.org/10.1080/1064119X.2016.1213337
45. Spagnoli G, Gavin K, Brangan C, Bauer S (2015) In situ and laboratory tests in dense sand investigating the helix-to-shaft ratio of helical piles as a novel offshore foundation system. In: Frontiers in offshore geotechnics III, no. MAY, CRC Press, pp 643–648
46. Spagnoli G, Jalilvand S, Kenneth G (2016) Installation torque measurements of helical piles in dry sand for offshore foundation systems. In: Geo-Chicago 2016 August 14–18, 2016, Chicago, Illinois, pp 439–448.
47. Spagnoli G, Tsuha CdHC (2020) A review on the behavior of helical piles as a potential offshore foundation system. Mar Georesour Geotechnol. https://doi.org/10.1080/1064119X.2020.1729905
48. Tagaya K, Scott FR, Aboshi H (1988) Scale effect in anchor pullout test by centrifugal technique. Soils Found 28(3):1–12
49. Tagaya K, Scott RF, Aboshi H (1988) Pullout resistance of buried anchor in sand. Soils Found 28(3):114–130
50. Tappenden K, Sego D (2007) Predicting the axial capacity of screw piles installed in Canadian soils. Can Geotech Soc (CGS) 1:1608–1615
51. Tatsuoka F, Goto S, Tanaka T, Tani K, Kimura Y (1997) Particle size effects on bearing capacity of footing on granular material. In: Deformation and progressive failure in geomechanics, IS-Nagoya. pp 133–138
52. Todeshkejoei C, Hambleton JP, Stanier SA, Gaudin C (2014) Modelling installation of helical anchors in clay. In: Proceedings of 14th international conference of the international association for computer methods and advances in geomechanics. pp 917–922. Doi: https://doi.org/10.1201/b17435-159.
53. Toyosawa Y, Itoh K, Kikkawa N, Yang J-J, Liu F (2013) Influence of model footing diameter and embedded depth on particle size effect in centrifugal bearing capacity tests. Soils Found 53(2):349–356. https://doi.org/10.1016/j.sandf.2012.11.027
54. Tsuha CdHC, Aoki N (2010) Relationship between installation torque and uplift capacity of deep helical piles in sand. Can Geotech J 47(6):635–647. https://doi.org/10.1139/T09-128
55. Tsuha CHC, Aoki N, Rault G, Thorel L, Garnier J (2007) Physical modelling of helical pile anchors. Int J Phys Model Geotech 7(4):01–12. https://doi.org/10.1680/ijpmg.2007.070401
56. Tsuha CHC, Santos TC, Rault G, Thorel L, Garnier J (2013) Influence of multiple helix configuration on the uplift capacity of helical anchors. In: 18th International conference on soil mechanics and geotechnical engineering: challenges and innovations in geotechnics, ICSMGE 2013, vol. 4. pp 2893–2896
57. Tsuha CdHC, Schiavon JA, Thorel L (2019) Evaluation of the breakout factor for helical anchors in sand by centrifuge testing. In: López-Acosta NP et al. (eds.) Geotechnical engineering in the XXI century: lessons learned and future challenges. Doi: https://doi.org/10.3233/STAL190128
58. Ullah SN, Hu Y, Loughlin CO (2019) A green foundation for offshore wind energy—helical piles. In: World Engineering Convention, WEC2019, Melbourne, Australia
59. Ullah SN, Hu Y, Stanier S, White D (2017) Lateral boundary effects in centrifuge foundation tests. Int J Phys Model Geotech 17(3):144–160. https://doi.org/10.1680/jphmg.15.00034

60. Victor RT, Cerato AB (2008) Helical anchors as wind tower guyed cable foundations. In: Proceedings of the second BGA international conference on foundations
61. Wang J, Haigh SK, Forrest G, Thusyanthan NI (2012) Mobilization distance for upheaval buckling of shallowly buried pipelines. J Pipeline Syst Eng Pract 3(4):106–114. https://doi.org/10.1061/(ASCE)PS.1949-1204.0000099

Terms and Conditions

Springer Nature journal content, brought to you courtesy of Springer Nature Customer Service Center GmbH (“Springer Nature”).
Springer Nature supports a reasonable amount of sharing of research papers by authors, subscribers and authorised users (“Users”), for small-scale personal, non-commercial use provided that all copyright, trade and service marks and other proprietary notices are maintained. By accessing, sharing, receiving or otherwise using the Springer Nature journal content you agree to these terms of use (“Terms”). For these purposes, Springer Nature considers academic use (by researchers and students) to be non-commercial.
These Terms are supplementary and will apply in addition to any applicable website terms and conditions, a relevant site licence or a personal subscription. These Terms will prevail over any conflict or ambiguity with regards to the relevant terms, a site licence or a personal subscription (to the extent of the conflict or ambiguity only). For Creative Commons-licensed articles, the terms of the Creative Commons license used will apply.
We collect and use personal data to provide access to the Springer Nature journal content. We may also use these personal data internally within ResearchGate and Springer Nature and as agreed share it, in an anonymised way, for purposes of tracking, analysis and reporting. We will not otherwise disclose your personal data outside the ResearchGate or the Springer Nature group of companies unless we have your permission as detailed in the Privacy Policy.
While Users may use the Springer Nature journal content for small scale, personal non-commercial use, it is important to note that Users may not:

1. use such content for the purpose of providing other users with access on a regular or large scale basis or as a means to circumvent access control;
2. use such content where to do so would be considered a criminal or statutory offence in any jurisdiction, or gives rise to civil liability, or is otherwise unlawful;
3. falsely or misleadingly imply or suggest endorsement, approval , sponsorship, or association unless explicitly agreed to by Springer Nature in writing;
4. use bots or other automated methods to access the content or redirect messages
5. override any security feature or exclusionary protocol; or
6. share the content in order to create substitute for Springer Nature products or services or a systematic database of Springer Nature journal content.

In line with the restriction against commercial use, Springer Nature does not permit the creation of a product or service that creates revenue, royalties, rent or income from our content or its inclusion as part of a paid for service or for other commercial gain. Springer Nature journal content cannot be used for inter-library loans and librarians may not upload Springer Nature journal content on a large scale into their, or any other, institutional repository.
These terms of use are reviewed regularly and may be amended at any time. Springer Nature is not obligated to publish any information or content on this website and may remove it or features or functionality at our sole discretion, at any time with or without notice. Springer Nature may revoke this licence to you at any time and remove access to any copies of the Springer Nature journal content which have been saved.
To the fullest extent permitted by law, Springer Nature makes no warranties, representations or guarantees to Users, either express or implied with respect to the Springer nature journal content and all parties disclaim and waive any implied warranties or warranties imposed by law, including merchantability or fitness for any particular purpose.
Please note that these rights do not automatically extend to content, data or other material published by Springer Nature that may be licensed from third parties.
If you would like to use or distribute our Springer Nature journal content to a wider audience or on a regular basis or in any other manner not expressly permitted by these Terms, please contact Springer Nature at

onlineservice@springernature.com